Available online at www.sciencedirect.com
SCIENCE DIRECT®
Journal of Solid State Chemistry 177 (2004) 3075–3079
JOURNAL OF SOLID STATE CHEMISTRY
http://elsevier.com/locate/jssc

Synthesis and photoluminescence of Eu^{3+}-doped $Y_2Sn_2O_7$ nanocrystals

Zhouguang Lu,[a,b] Junwei Wang,[a] Yougen Tang,[b] and Yadong Li[a,*]

[a] *Department of Chemistry, Tsinghua University, Beijing 100084, People's Republic of China*
[b] *Collage of Chemistry and Chemical Engineering, Central South University, Changsha, Hunan 410083, People's Republic of China*

Received 21 November 2003; received in revised form 28 March 2004; accepted 26 April 2004

Abstract

A facile CTAB-assisted sol–gel route has been successfully established to synthesize $Y_2Sn_2O_7$ nanocrystals with pyrochlore structure. The route involves first the formation of CTAB-inorganics mesostructures as precursors and then their thermal decomposition to yield the final product. Well-crystallized and phase-pure $Y_2Sn_2O_7$ particles of $\sim$40 nm in size can be readily obtained at 600°C, a temperature much lower than that of the conventional solid-state method. Furthermore, photoluminescence characterization of the $Y_2Sn_2O_7$ nanocrystals doped with 5 mol% Eu^{3+} was carried out and the results show that the as-synthesized material display intense and prevailing emission at 589 nm belonging to the $^5D_0 \rightarrow {}^7F_1$ magnetic dipole transition.

Keywords: Yttrium stannate; Europium; Pyrochlore; Nanocrystals; CTAB-assisted sol–gel; Photoluminescence

1. Introduction

Pyrochlore oxides have the chemical composition $A_2B_2O_7$, where the A and B atoms are metals located on the sites 16*d* and 16*c*, respectively. The basic framework of the pyrochlore structures is a three-dimensional corner-sharing network of MO_6 octahedra [1,2]. Of the various pyrochlore oxides the rare earth stannates, $Ln_2Sn_2O_7$ (Ln = Y, La–Lu), form a group of isostructural compounds and consequently have been well investigated [3]. The series of stannates pyrochlore oxides shows a variety of interesting electrical and magnetic properties, that is, of particular technological importance for numerous applications including catalysis, piezoelectricity, ferro- and ferrimagnetism, giant magnetoresistance, resistance to radiation damage and so forth [1–6]. There has been a growing interest in strong luminescence of europium ions activated nanocrystals due to their promising applications in fluorescent lamps [7], field emission display [8] and plasma display panels [9]. Nevertheless, the list of such phosphors, extensively discussed in literature, is almost exhausted by the following systems: Y_2O_3:Eu^{3+} [7], YBO_3:Eu^{3+} [10], and YVO_4:Eu^{3+} [11]. Here a novel phosphors using stannate pyrochlore oxides as host materials ($Y_2Sn_2O_7$:Eu^{3+}) displaying strong fluorescence, are synthesized and its relationship between crystal structure and emission properties are also definitely reported.

The existing methods for the preparation of stannate pyrochlores are fairly cumbersome, as it employs a solid-state reaction of SnO_2 with appropriate yttrium oxide at high temperature (ca. 1500°C) for a very long time (ca. 5 days). In this paper we have successfully established a simple Cetyltrimethyl Ammonium Bromide (CTAB)-assisted sol–gel technique to prepare phase-pure yttrium tin pyrochlore ($Y_2Sn_2O_7$) nanocrystals. This method adopts a calcinations temperature as low as 600°C. Furthermore, these nanocrystals are functionalized by introducing Eu^{3+} ions into the crystal lattice, which endows the nanocrystals luminescent properties and provides new fascinating opportunities for phosphor applications.

2. Experiments

2.1. Samples preparation

$SnCl_4 \cdot 5H_2O$ (7.02 g) was dissolved in 30 mL distilled deionized water (DDW) and heated to 80°C.

*Corresponding author. Fax: +86-10-62788765.
E-mail address: ydli@tsinghua.edu.cn (Y. Li).

0022-4596/$ - see front matter © 2004 Elsevier Inc. All rights reserved.
doi:10.1016/j.jssc.2004.04.053

Table 1
Heat-treatment conditions and corresponding results

Samples	*a*	*b*	*c*	*d*	*e*	*f*	*g*	*h*
Heat treatment conditions[a]	400°C for 3 h	600°C for 3 h	800°C for 3 h	900°C for 3 h	1000°C for 3 h	1100°C for 3 h	1200°C for 3 h	1300°C for 3 h
R_{TEM}[b]	—	40 nm	90 nm	140 nm	200 nm	820 nm	1.3 μm	2 μm

[a] Heating rate is fixed at 10°C/min.
[b] R_{TEM} represents the statistical crystal diameter obtained from the results of transmission electron microscopy (TEM) measurement.

Appropriate amount of 2 M NaOH solution was added to the $SnCl_4$ solution under vigorous stirring to completely precipitate Sn^{2+} and form $Sn(OH)_4$ slurry. Separately, 2.26 g Y_2O_3 was first dissolved by hot concentrated nitric acid to produce $Y(NO_3)_3$ solution and then $Y(OH)_3$ slurry was obtained similar to the formation of $Sn(OH)_4$. Then the two slurries were mixed thoroughly by vigorous stirring and the pH of the mixture was adjusted at ca. 10 by 1 M NaOH or 0.5 M HNO_3 solutions. A 30% aqueous surfactant solution of CTAB (14.6 g in 50 mL DDW) was added to the $Sn(OH)_4$ and $Y(OH)_3$ mixture and the pH of the mixture was controlled at 12. The mixture was stirred at 80°C for 5 h and then heated at 80°C for 24 h. The supernatant was then decanted, and the solid residue was washed six times with alcohol and DDW, respectively, dried in air at ambient temperature. The as-prepared precursors were annealed at different conditions as summarized in Table 1. The Eu^{3+}-doped $Y_2Sn_2O_7$ samples were prepared slightly differently, just replacing 5 mol% amount of Y_2O_3 by Eu_2O_3.

2.2. Samples characterization

The XRD data were collected using a Japan Rigaku Dmax rA X-ray diffractionmeter with graphite monochromatized Cu$K\alpha$ radiation ($\lambda = 1.5418$ Å). The morphology of the final products was characterized with a Hitachi H-800 transmission electron microscope (TEM) operated at 200 kV. The photoluminescence measurements were carried out using a Hitachi F-4500 fluorescence spectrophotometer. The excitation spectra were corrected for the beam intensity variation in the Xe light-source used.

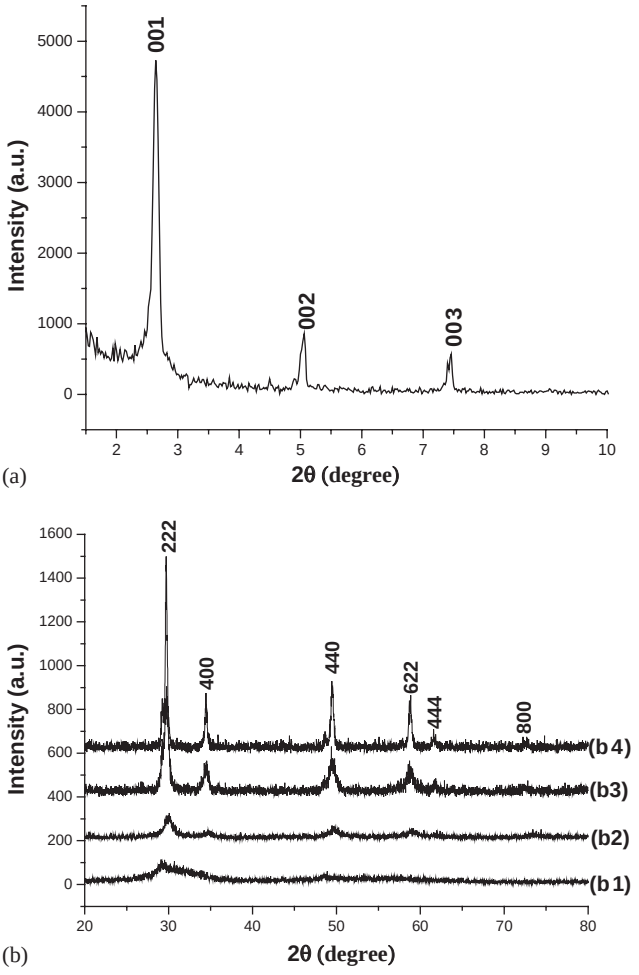

Fig. 1. (a) Low-angle XRD patterns of the as-synthesized mesostructure CTAB-inorganic precursor; (b) Wide-angle XRD patterns of the as-produced samples annealed for 3 h at the temperature of: 400°C (b1), 600°C (b2), 1000°C (b3) and 1300°C (b4), respectively. The high-angle diffractions are indexed according to the corresponding cubic pyrochlore-structured $Y_2Sn_2O_7$ phases.

3. Results and discussion

3.1. Formation of phase-pure $Y_2Sn_2O_7$ particulates

The low-angle XRD pattern of the as-synthesized precursors is characterized by three diffraction peaks at $2\theta = 1-10^\circ$ as shown in Fig. 1a. The three peaks can be attributed to the 001, 002 and 003 reflections for a typically layered mesostructure, suggesting that CTA^+ molecules would be arranged as a bilayer between the inorganic layers [12]. However, the low angle XRD reflections disappear above 400°C, indicating the unstability of the mesostructure. Fig. 1b shows the wide-angle XRD patterns of the samples after calcinations with different temperature. It is clear from Fig. 1(b1) that the sample annealed at 400°C for 3 h are amorphous, which is further confirmed by TEM image in Fig. 2a and selected area electron diffraction

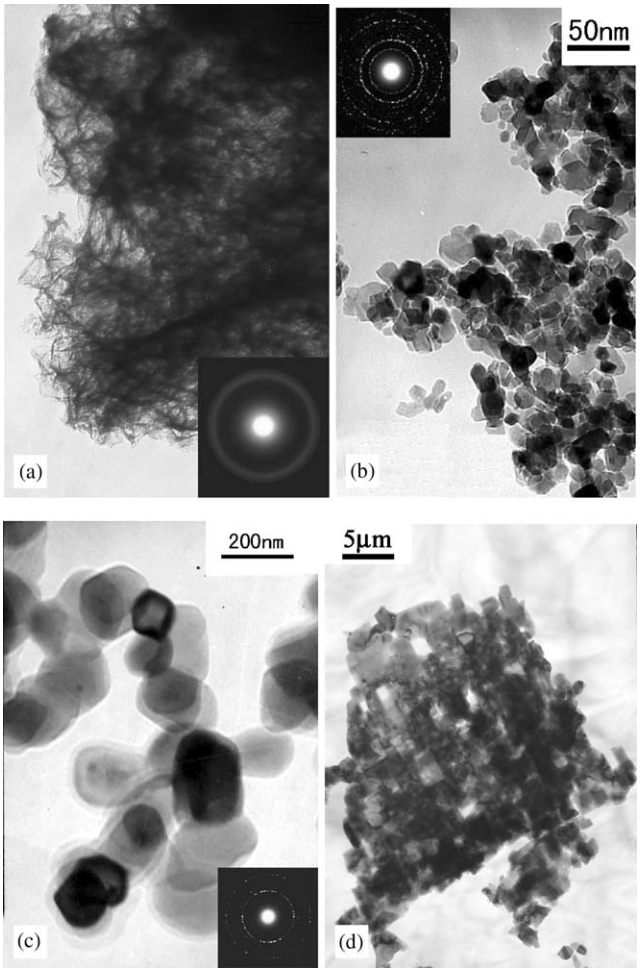

Fig. 2. Typical TEM images of the samples annealed at: 400°C (a), 600°C (b), 1000°C (c) and 1300°C (d), respectively. Insets are corresponding selected-area electron diffraction (SAED) patterns.

(SAED) pattern as shown therein. Fig. 1(b2) represents the XRD pattern of the sample after heat-treatment at 600°C for 3 h and it is evident that all diffraction lines can be readily indexed to a pure cubic phase $Y_2Sn_2O_7$ with pyrochlore structure conforming to the *Fd*3*m* space group (JCPDS 731684). But all the peaks are broadened due to reduced crystal size. The TEM image of this sample as expressed in Fig. 2b, together with SAED patterns as shown in inset, indicates that well-crystallized $Y_2Sn_2O_7$ particles with a mean diameter of 40 nm can be successfully obtained at 600°C, a temperature much lower than that adopted by the conventional solid-state method. Moreover, the particles are fairly uniform both in shape and size. Fig. 1(b3) and Fig. 1(b4) display XRD images of the particles annealed at 1000°C and 1300°C, respectively. From these XRD patterns it can be concluded that the integral peak intensity are stronger and the full-width at half-maximum (FWHM) is narrower with calcination temperature. Figs. 2c and d present typical TEM images of the samples annealed at 1000°C and 1300°C, respectively. It shows that clear-shape and comparatively weakly agglomerated $Y_2Sn_2O_7$ crystals with a mean diameter of 200 nm are produced at the annealing conditions of 1000°C for 3 h. However, when the temperature increases to 1300°C, the particles grow, drastically aggregate and become irregular in shape. These demonstrations suggest that increasing annealing temperature results in higher crystallinity and larger crystal size, but a too high temperature deteriorates the crystal uniformity.

How are atoms or other building blocks assembling into such single crystal $Y_2Sn_2O_7$ nanoparticles in this CTAB-assisted sol–gel approach without any impure phase segregation? Based on the works of Huo QS et al. [13], a mechanism is proposed as schematically represented in Fig. 3. The process can be mainly divided into four steps. (1) The CTA^+ cations condense into aggregates in which the $[Y(OH)_6]^{3-}$ and $[Sn(OH)_6]^{2-}$ anions are intercalated homogeneously in the interspaces between the head groups of CTA^+ to form $CTA–Y(OH)_6–Sn(OH)_6$ ion complexes. (2) The continuing condensation process generates more highly ordered mesolamellar assemblies, which are confirmed by low-angle X-ray diffraction in Fig. 1a. (3) When heated in air to certain temperature, these lamellar sheets begin to collapse. (4) With gradually increasing temperature, as the degradation of CTA^+ organic phase, the adjoining molecular species aggregate, grow and finally nucleate into phase-pure $Y_2Sn_2O_7$ nanoparticles. In this CTAB-assisted sol–gel process, tin and yttrium can be compositionally assembled in the mesoporous structure and during the annealing stage, the lamellar framework is first broken and CTA-inorganic fragments are consequently produced as elucidated in Fig. 3(1) and evidenced by Fig. 2a. And as the proceeding of calcinations, decomposition of organic phase and crystallization of inorganic phase progress simultaneously, which can effectively avoid the isolation of Y_2O_3, SnO_2 or any other impure phases. Therefore, the formation of intermediate mesolamellar structure is the essence of this CTAB-assisted sol–gel technique in the preparation of phase-pure $Y_2Sn_2O_7$ particulates.

To substantiate our hypothesis, we performed control experiments. Sn^{4+} and Y^{3+} ions were appropriately coprecipitated without subsequent interaction with CTAB surfactant. No lamellar composite structures were present in these as-synthesized composites according to low-angle XRD data (not shown). Fig. 4 shows the representative XRD patterns of the final products synthesized by using CTAB or not. Obviously, without the subsequent interaction with surfactant, three series of peaks according to the phases of $Y_2Sn_2O_7$, Y_2O_3 and SnO_2 as marked are comprised in it (Fig. 4b). Moreover, the diffractions of the desired $Y_2Sn_2O_7$ phase are fairly weak. That is to say, under the same experimental conditions, it fails to prepare monophase $Y_2Sn_2O_7$

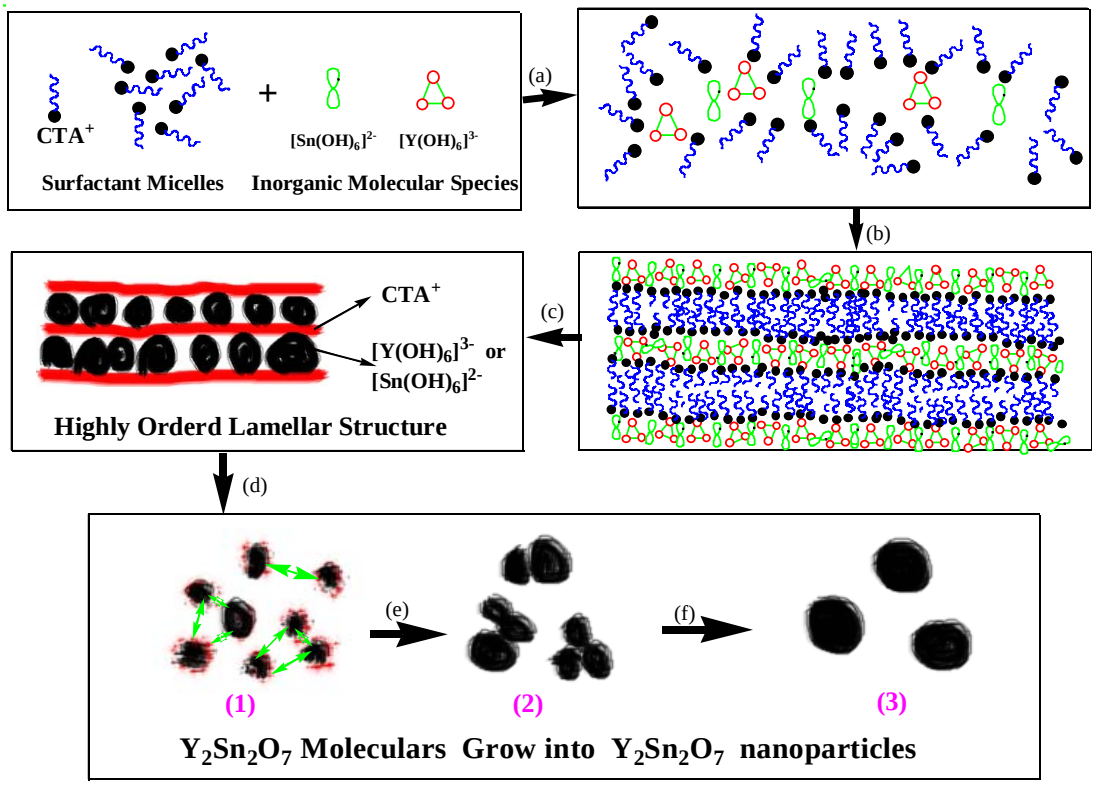

Fig. 3. Schematic representation of different periods in the CTAB-assisted sol–gel preparation of phase-pure $Y_2Sn_2O_7$ particulates. (a) Cooperative nucleation; (b) liquid crystal formation with molecular inorganic compounds; (c) organic–inorganic polymerization and condensation; (d) collapsing of surfactant-inorganic mesostructure into separate molecular species; (e) degradation of the organic phase and inclination of agglomeration; and (f) molecular species growing into nanoparticulates.

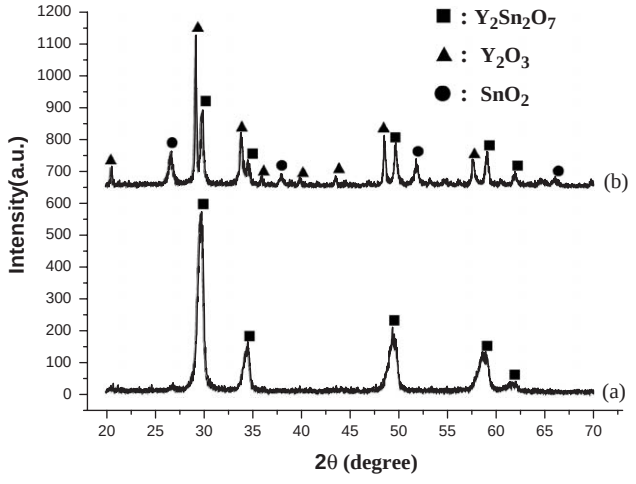

Fig. 4. Typical XRD patterns of the as-synthesized samples with (a) or without (b) the subsequent interaction with CTAB. All samples are annealed at 1000°C for 3 h in air. The marks of cube, up triangle and circle represent phases of $Y_2Sn_2O_7$, Y_2O_3 and SnO_2, respectively.

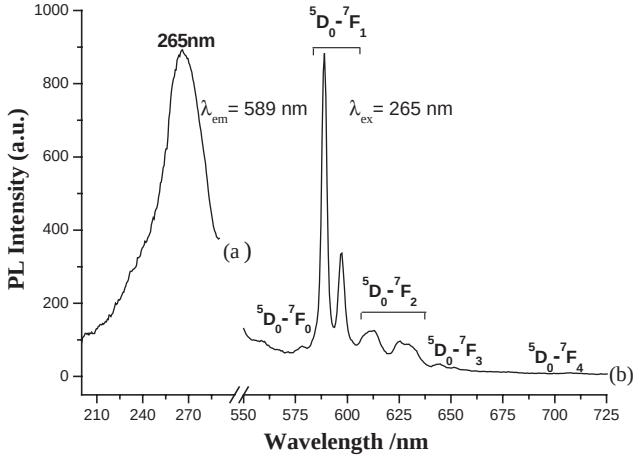

Fig. 5. Typical room temperature excitation (for the emission at 589 nm) (a) and emission (excited by 265 nm) (b) spectra of the as-synthesized $Y_2Sn_2O_7$:Eu^{3+} (5% molar ratio) nanocrystals.

without the introducing of surfactant. It is supposed that Sn^{4+} and Y^{3+} ions cannot be effectively and well-proportionally coprecipitated due to their large physicochemical difference. As a result, phase isolation happens during the process of calcinations. Whereas the preassembling of CTAB-inorganic mesostructure can solve this problem.

3.2. *Photoluminescence characterization of Eu^{3+} ions*

Fig. 5 shows representative room temperature photoluminescence excitation (PLE) and emission (PL)

spectra of the as-synthesized $Y_2Sn_2O_7$:Eu^{3+} nanocrystals. The excitation spectrum (Fig. 5a) exhibits broad band between 200 and 300 nm, which can be attributed to charge transfer band between the Eu^{3+} and the surrounding oxygen anions [14–16]. The emission spectrum (Fig. 5b) consists of profiles mainly located in the red spectral area (from 575 to 630 nm), corresponding to transition from the excited $^5D_0$ state to ^7F_J ($J=0,1,2,3,4$) levels of $4f^6$ configuration of Eu^{3+} [15]. The $4f$ energy levels of Eu^{3+} are hardly affected by the crystal field because of the shielding effect of the $5s^25p^6$ electrons. However, the selection rules and transition probabilities between states strongly depend on the crystal field. When the Eu^{3+} ions embedded in a site with inversion symmetry, the $^5D_0 \rightarrow {}^7F_1$ magnetic dipole transition is dominating, while in a site without inversion symmetry the $^5D_0 \rightarrow {}^7F_2$ electric dipole transition is the strongest [15,17,18]. Therefore the fluorescence intensity ratio of $^5D_0 \rightarrow {}^7F_2$ to $^5D_0 \rightarrow {}^7F_1$, called as asymmetry ratio, gives a measure of the degree of distortion from inversion symmetry of the local environment around the Eu^{3+} ions in the host matrix [17,18]. One can see from the emission spectrum of the as-synthesized $Y_2Sn_2O_7$:Eu^{3+} nanocrystals (Fig. 5b) that the most intense peak centers at 589 and 597 nm. Both peaks correspond to the magnetic dipole transitions between the $^5D_0$ and $^7F_1$ levels and are much stronger than that of the $^5D_0 \rightarrow {}^7F_2$ (centered at 612 and 625 nm) transitions, revealing good monochromaticity of the resulting $Y_2Sn_2O_7$:Eu^{3+} materials and a inversion symmetry environment for the Eu^{3+} sites in the host lattice. In the pyrochlore $Y_2Sn_2O_7$, the Y atom is coordinated to eight oxygen and the Sn atom is surrounded by six oxygen in a geometry only slightly distorted from a regular octahedron. To the best of our knowledge, both cation sites have inversion symmetry [1–3,19]. Unambiguously, the prevailing $^5D_0 \rightarrow {}^7F_1$ emission in the observed emission spectrum (Fig. 5b) is well consistent with the geometric circumstances of the Eu^{3+} sites (substituting Y^{3+}) in the pyrochlore structure.

4. Conclusion

In summary, $Y_2Sn_2O_7$ nanocrystals can be readily synthesized by a simple Cetyltrimethyl Ammonium Bromide (CTAB)-assisted sol–gel approach. As synthesized, the material is mesoporous as precursors. Annealing the precursors at 400°C results in the collapse of the mesostructure and at 600°C results in well-crystallized and phase-pure pyrochlore $Y_2Sn_2O_7$ nanocrystals with a grain size of ~40 nm. After doped with 5 mol% Eu^{3+} ions in the Y^{3+} sites, the $Y_{2-x}Eu_xSn_2O_7$ material displays intense emissions in the red area (from 575 to 630 nm) with their strongest line at 589 nm corresponding to the $^5D_0 \rightarrow {}^7F_1$ magnetic dipole transition.

Acknowledgments

This work was supported by the NSFC (20025102, 50028201,20151001), the Foundation for the Author of National Excellent Doctoral Dissertation of P.R. China, and the State Key Project of Fundamental Research for nanomaterials and nanostructures.

References

[1] J.N. Reimers, J.E. Greedan, J. Solid State Chem. 72 (1988) 390.
[2] H. Mizoguchi, H.W. Eng, P.M. Woodward, Inorg. Chem. 43 (2004) 1667.
[3] B.J. Kennedy, B.A. Hunter, C.J. Howard, J. Solid State Chem. 130 (1997) 58, and references therein.
[4] K.E. Sickafus, L. Minervini, R.W. Grimes, J.A. Valdez, M. Ishimaru, F. Li, K.J. Mcclellan, T. Hartmann, Science 289 (2000) 748.
[5] M.D. Lumsden, S.R. Dunsiger, J.E. Sonier, R.I. Miller, R.F. Kiefl, R. Jin, J. He, D. Mandrus, S.T. Bramwell, J.S. Gardner, Phys. Rev. Lett. 89 (2002) 147002.
[6] S. Park, H.J. Hwang, J. Moon, Catal. Lett. 87 (2003) 219.
[7] S.W. Kang, J.S. Yoo, J.D. Lee, J. Electrochem. Soc. 145 (1998) 648.
[8] D.K. Wilams, B. Bhihari, B.M. Tissue, J. Phys. Chem. B. 102 (1998) 916.
[9] O.A. Serra, S.A. Cicillini, R.R. Jshiki, J. Alloys Compound 303–304 (2000) 316.
[10] X.C. Jiang, C.H. Yan, L.D. Sun, Z.G. Wei, C.S. Liao, J. Solid State Chem. 175 (2003) 245.
[11] A. Huignard, V. Buissette, G. Laurent, T. Gacoin, J.P. Boilot, Chem. Mater. 14 (2002) 2264.
[12] Z.R. Tian, W. Tong, J.Y. Wang, N.G. Duan, V.V. Krishnan, S.L. Suib, Science 276 (1997) 926.
[13] Q.S. Huo, D.I. Margolese, U. Ciesla, D.G. Demuth, P.Y. Feng, T.E. Gier, P. Sieger, A. Firouzi, B.F. Chmelka, F. Schuth, G.D. Stucky, Chem. Mater. 6 (1994) 1176.
[14] R. Schmechel, M. Kennedy, H.V. Seggern, H. Winkler, M. Kolbe, R.A. Fischer, X.M. Li, A. Benker, M. Winterer, H. Hahn, J. Appl. Phys. 89 (2001) 1679.
[15] G. Blasse, B.C. Geiabmaier, Luminescent Materials, Springer, Berlin, 1994, p. 117.
[16] G. Wakefield, E. Holland, P.J. Dobson, J.L. Hutchison, Adv. Mater. 13 (2001) 1557.
[17] B.R. Judd, Phys. Rev. 127 (1962) 750.
[18] G.S. Ofelt, J. Chem. Phys. 37 (1962) 511.
[19] http://www.chemistry.ohio-state.edu/~woodward/ch754/struct/pyrochlore.htm.